The use of Plasma Mirror for Relativistic Electron Generation Relevant to Fast Ignition in Inertial Confinement Fusion

David Moiraf
3rd year Special Program Bachelor in Physics, Paul Sabatier University, Toulouse, FR

Mentors:
Prof. Alessio Morace (morace@ile.osaka-u.ac.jp)
Prof. Yasunobu Arikawa (arikawa-y@ile.osaka-u.ac.jp)
Fusion Plasma Science Group, Institute of Laser Engineering, Osaka University, Osaka, JP

May 2020

Abstract

We are becoming dependent on energy more today than we were a century ago, and with increasing world population and booming economies, sooner or later our energy sources will be exhausted. Moreover, our economy and welfare strongly depend on foreign oil and in the shadow of political uncertainties, there is an urgent need for a reliable, safe, and cheap energy source. Thermonuclear fusion, if achieved, is that source of energy which not only will satisfy our demand for today but also for centuries to come. Today, there are two major approaches to achieve fusion: magnetic confinement fusion (MFE) and inertial confinement fusion (ICF). This dissertation explores the inertial confinement fusion using the fast ignition concept (FI) and the cone-in-shell method. Unlike the conventional approach where the same laser is used for compression and ignition, here, two separate laser beams are being used. Here, we will focus on the ignitor beam, generated by the LFEX, the most powerful laser in the world. This beam is a picoseconds pulse reaching an intensity greater than $10^{19}\ W/cm^2$, used to generate relativistic electrons from the cone target to the imploding fuel core, giving it the energy necessary to initiate the thermonuclear reaction. However, picoseconds laser pulses are preceded by a pedestal of few nanoseconds and several orders of magnitude lower intensity than the main picoseconds one, preventing the generation of an ideal hot electron beam. This dissertation will show how a pedestal can affect the relativistic electron generation, and how Plasma Mirrors (PM) can be used in order to improve the beam contrast, thus increasing the energy absorption of the fuel core. We will also see how we setup the PM for the fusion chamber of the Institute of Laser Engineering of the Osaka University.

Acknowledgements

I would like to thank everyone who participated in the creation and maintenance of the Paul Sabatier Special Program. With this course, I had the opportunity to go abroad and carry out my internship in a country that I always dreamed to visit. Thank to Prof. Pettinari-Sturmel, who accompanied me throughout the internship search and the paper work.

Thank to the CROUS Toulouse, the Paul Sabatier University and the Région Occitanie for covering my expenses during my internship in Japan.

A big thanks to the ILE and the FPS group for their warm welcome in their team. I want to specially thank my mentors Prof. Yasunobu and Prof. Morace, who had the patience to carry me throughout my project and gave several hours of their day to explain to me how things work.

Thank to all the people that helped me and taught me the culture and traditions of this beautiful country that is Japan. This is for you Shunsuke, Hotaka, Nathan, Benjamin and Roy.

To the Narmamènes and the Tocards for always being there and fill my heart with joy.

Finally, I want to thank my family for always supporting my dreams.

I do not thank the Coronavirus.

Contents

1 Introduction **4**
- 1.1 Nuclear Fusion . . . 4
- 1.2 Principles of Inertial Confinement Fusion (ICF) . . . 6
- 1.3 Cone-guided Fast Ignition concept (FI) . . . 6
- 1.4 Electron temperature distribution . . . 7
- 1.5 Motivation for using Plasma Mirrors (PM) . . . 8

2 Review of theory of laser-plasma interaction **10**
- 2.1 Equations derived from the plasma physics . . . 10
- 2.2 Single electron in a laser field . . . 11
- 2.3 Laser interaction with under-dense plasma . . . 12
  - 2.3.1 Self-focusing and filamentation . . . 12
  - 2.3.2 Inverse Bremsstrahlung . . . 13
- 2.4 Laser interaction with over-dense plasma . . . 14
  - 2.4.1 Resonance absorption . . . 14
  - 2.4.2 Vacuum heating . . . 15
  - 2.4.3 J x B heating . . . 15
- 2.5 Electron beam transport through plasma . . . 15
  - 2.5.1 Conversion efficiency . . . 15
  - 2.5.2 Stopping power . . . 16
  - 2.5.3 Plasma resistivity . . . 16

3 Computational study **18**
- 3.1 Particle-In-Cell model (PIC) . . . 18
- 3.2 2D simulation of high intensity laser interaction with pre-formed plasma . . . 19
- 3.3 Results . . . 19
  - 3.3.1 Effect on conversion efficiency . . . 19
  - 3.3.2 Effect on fast electron divergence . . . 21
- 3.4 Conclusion on heating performance . . . 22

4 Setup and Installation of the Plasma Mirror (PM) **23**
- 4.1 Introduction . . . 23
  - 4.1.1 Constraints . . . 23
- 4.2 Work at the Alignment Station (AS) . . . 23
  - 4.2.1 Target Chamber Center (TCC) . . . 23
  - 4.2.2 LFEX skeleton . . . 24
  - 4.2.3 Mirror Alignment . . . 25

5 Conclusion and perspective **26**
- 5.1 Summary and conclusions . . . 26
  - 5.1.1 Fast electron generation and transport . . . 26
  - 5.1.2 Effect of pre-formed plasma for fast electron generation . . . 26
  - 5.1.3 Setup and Installation of the plasma mirror . . . 26
- 5.2 Future Work . . . 26
- 5.3 Personal review . . . 27

1 Introduction

1.1 Nuclear Fusion

Fusion occurs when two light nuclei combine into a heavier nucleus. Because the mass of the heavier nucleus is smaller than the sum of the mass of the two light nuclei, the missing mass is released as energy, and the reaction is exothermic. The quantity of energy released follow the famous Einstein's special relativity result:

$$\triangle E = \triangle m \; c^2 \tag{1}$$

Where $\triangle m$ is the the mass difference between the products and reactants, and c is the speed of light in vacuum. The energy released when the neutrons and protons combine to form the nucleus is called the binding energy of the nucleus. The figure 1 plot the binding energy per nucleon as function of the mass number A. It appears clear that it is possible to produce nuclear energy by dividing high Z nuclei (fission) or fusing together low Z nuclei (fusion).

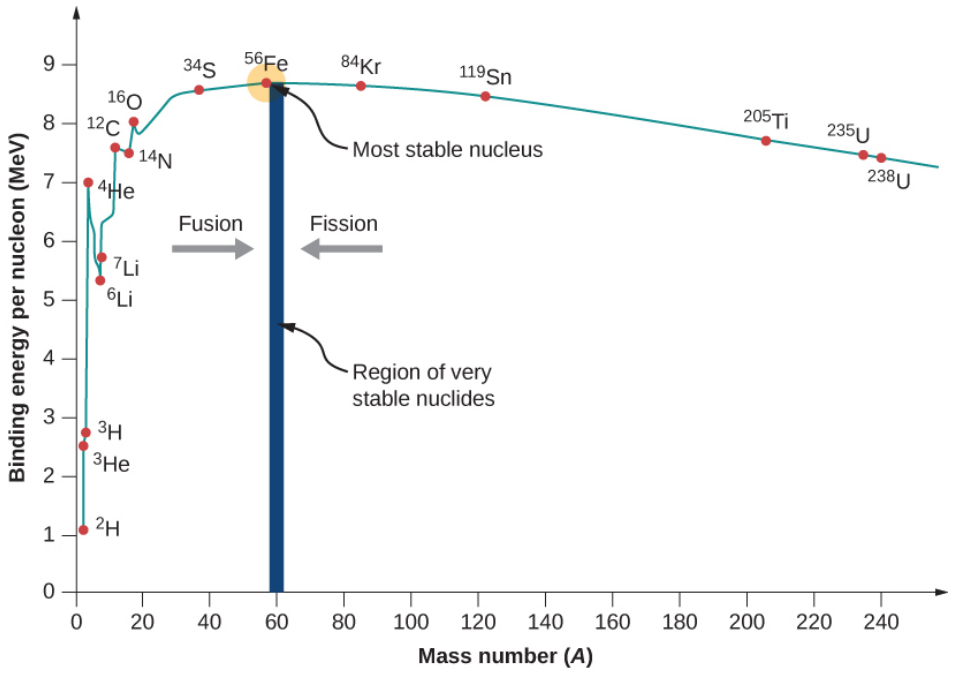

Figure 1: Binding energy per nucleon versus atomic mass number A.

Up to now, the only source of nuclear energy has been represented by fission of U_{235} nuclei in nuclear power plants. In France, nuclear power plants represents 71.6% (379,1 TWh) of the electricity production in 2017 according to the RTE. This is the highest percentage in the world. Despite the great advantages of fission power plants in terms of amount of energy produced, strong reduction in air pollution and greenhouse gas production, several are the problems related to this source of energy. The limited reserve of uranium guarantees energy production at the actual rate for no more than 100 years, and the large quantity of nuclear waste produced represents a serious concern in terms of stoking and related safety.
Nuclear fusion instead, produces no nuclear waste except for some neutron stimulated nuclear activation of the interaction chamber walls. Moreover it is intrinsically safe and, being hydrogen the most common element in the Universe, it represents a quasi-endless supply of fuel for fusion energy.

In order for two nuclei to fuse they must be brought close to each other such that the strong nuclear force dominates the repulsive Coulomb force. The maximum Coulomb potential is given by:

$$V_c = \frac{Z_1 Z_2 e^2}{r_n} \tag{2}$$

where Z_1 and Z_2 are the nuclear charges and r_n is the inter-nuclei distance. Since this Coulomb force preventing two nuclei from getting closer is an increasing function of the atomic number Z, the most promising fusion reactions are those involving Hydrogen and its isotopes. The cross section $\sigma(v)$ represents the probability of the reaction event per pair of ions. The probability of reaction per unit time is given by $n\sigma(v)v$. Another very important quantity is the fusion reactivity, which is defined as the probability of reaction per unit time and unit density of target nuclei. Assuming a normalized velocity distribution f(v) for the interacting nuclei, we can define the average fusion reactivity as:

$$\langle \sigma v \rangle = \int_0^\infty \sigma(v) v f(v) dv \tag{3}$$

The volumetric reaction rate is given by:

$$R_{12} = \frac{f_1 f_2}{1 + \delta_{12}} n^2 \langle \sigma v \rangle \tag{4}$$

where the indices 1 and 2 indicate the two reacting ion species and δ_{ij} is the Kronecker symbol. If we plot the fusion cross sections versus ion temperature in eV for various fusion reaction, we can remark that the Deuterium and Tritium (DT) have the biggest cross section for a relatively low temperature (see figure 2).

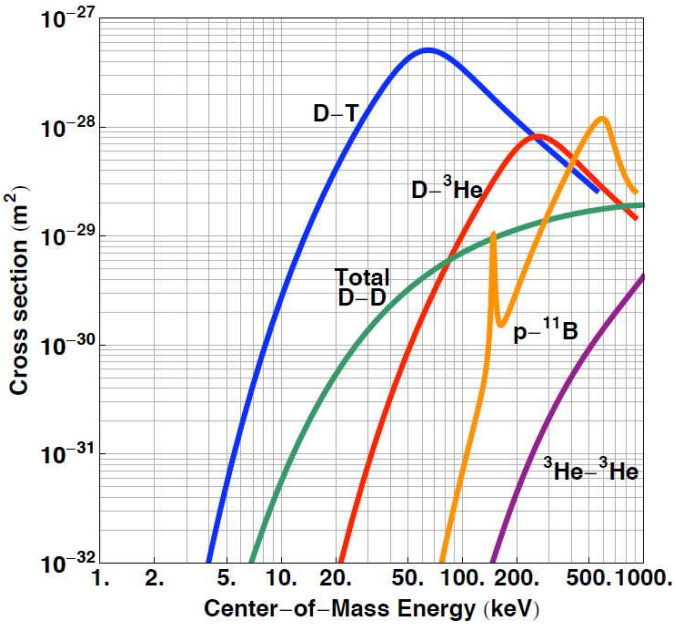

Figure 2: Fusion cross sections for various fusion reaction versus ion temperature. The DT fusion cross section is the largest at low temperatures.

This is why we use the DT-reaction in the Institute of Laser Engineering:

$$D \ + \ T \ \rightarrow \ \alpha(3.5 \ MeV) \ + n(14.1 \ MeV) \tag{5}$$

This reaction releases a total of 17.6 MeV per fusion reaction, the most of it carried by the neutron, while the α particle energy, responsible for the plasma heating, guarantees the reaction to be self sustained. We use electron-volt (eV) because it is more convenient than joule when we are dealing with atoms and nuclei to express the energy ($1eV = 1.602 \times 10^{-19} J \sim 11\ 604.45\ K$).
To achieve self sustained nuclear fusion reactions, the α particle heating rate must be larger than the power loss rate. The Lawson criteria compares the rate of energy being generated by fusion reactions within the fusion fuel to the rate of energy losses to the environment [1]. When the rate of production is higher than the rate of loss, and enough of that energy is captured by the system, the system is said to be ignited. If this criteria is respected, the system achieve self sustained nuclear fusion reactions.

1.2 Principles of Inertial Confinement Fusion (ICF)

Unlike magnetic fusion where low densities and long confinement times are used to satisfy the Lawson criterion, in ICF high densities and short confinement times are used to achieve the same goal. The high densities can be achieved by compressing the fuel using lasers or ion beams. The inertia of the imploding fuel keeps it together, long enough, for ignition and burn to happen. This is why we call it "Inertial confinement fusion". This is the same process used in hydrogen bombs, however achieving it in a controlled fashion result to be a difficult task.

The target is composed by a solid layer of spherical DT ice (that we will call the capsule), surrounding DT gas. In order to compress the fuel, it exist two primary schemes for which the lasers can provide the necessary energy: (1) direct drive, in which lasers are directly incident on the fuel capsule, driving the implosion with their radiation pressure (see section 2.3.2), and (2) indirect drive, where the lasers are first incident on a hohlraum (a high-Z cylindrical enclosure, mainly made out of Au) which produces x-rays that irradiate the fuel capsule (see figure 3). The direct drive method is more efficient in term of energy loss, because the laser hit directly the fuel. But with the indirect drive, we assure a more symmetrical compression.

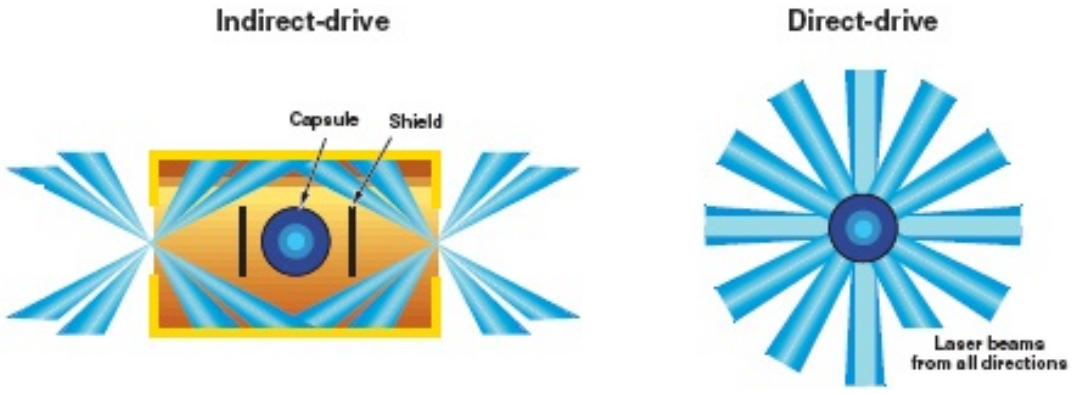

Figure 3: Indirect drive (left) and Direct drive (right).

The energy of the lasers is given to the capsule that will expand, and so, compress the DT gas by the rocket-like blow-off, compressing and heating the fuel via shocks and PdV work.

1.3 Cone-guided Fast Ignition concept (FI)

If we rely on the implosion alone to produce ignition, we are creating a Central Hot Spot (CHS). This is the most developed method of ignition, used in the National Ignition Facility (NIF), being currently the

biggest operational ICF institute. CHS ignition minimizes the driver energy needed for ignition by using the highest possible pressure, leading to the high density of the main fuel. However, since the Fermi energy scales as $\rho^{2/3}$, more energy per unit of mass is invested into the compression of the fuel in spite of the heating of the hot spot. Furthermore, it is complicated to have a very symmetrical compression, because of hydrodynamic instabilities and the formation of a 'tight' shock wave convergence at the compressed fuel center.

The Fast Ignition (FI) concept gets around the problem by igniting a small region of the main fuel at the same density as shown in the figure 4. The hot spot is created using a secondary, ultra-intense picosecond laser. The FI pulse duration must be lower than the inertial confinement time governed by the radius of the hot spot, which is $\sim 20\ ps$ for a density of $\sim 300\ g\ cm^{-3}$. In the ILE, the compressor beam is assured by the GEKKO XII laser, and the ignitor beam is assured by the LFEX laser.

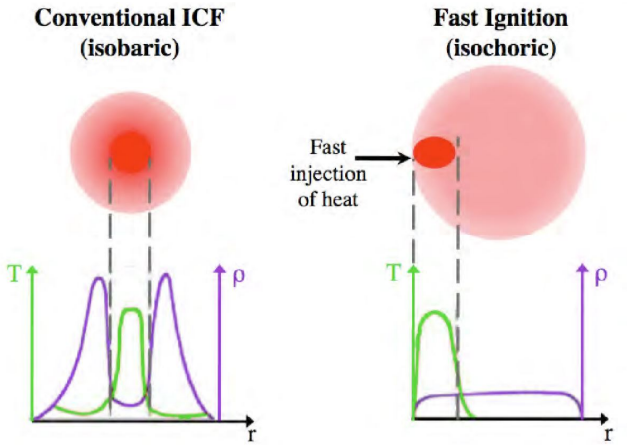

Figure 4: Fuel assembly for CHS ignition (isobaric assembly), and Fast Ignition (isochoric assembly).

For the cone guided concept, the ignitor beam will be focused on a target that will generate hot electrons. Theses particles will heat our main fuel thanks to collisional heating, creating the hot spot. As a result, the gain can be higher and the ignition threshold lower as shown on the figure 5. The cone serves two purposes: (1) It protect the ignitor beam from the exploding plasma from the capsule, as this under-dense plasma have an effect on the laser (see section 2.3). (2) It generate and transport hot electrons to the imploded fuel core at the tip of the cone (see section 2.4). The figure 6 present a photography of an actual target for cone-guided FI.

1.4 Electron temperature distribution

To understand our problem, we need to clarify the concept of "temperature". In literature, the definition of fast electron "temperature" is sometimes quite confused, and in some cases, should be substituted with the term of "average energy". The fast electron energy distribution can be described as an exponential, or a composition of exponential distributions of the form

$$f(E) \approx e^{-E/T_{hot}} \tag{6}$$

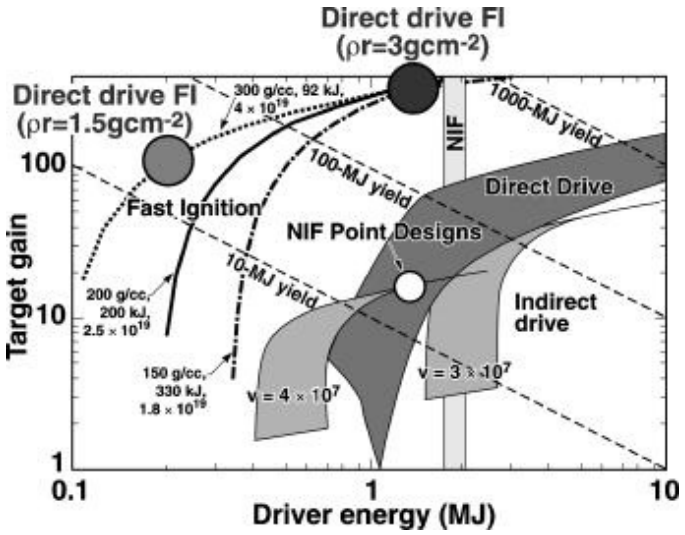

Figure 5: Gain estimates for direct-drive Fast Ignition targets from a simple analytic model compared with numerically modeled CHS ignition disigns for NIF. The FI gain curves are labeled with fuel density, energy, and $I\lambda^2$ in the ignitor laser beam, assuming a wavelength of 530nm. [2]

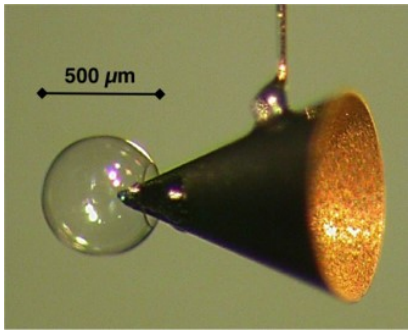

Figure 6: Au cone target from the ILE, Osaka University.

where T_{hot} is the slope-temperature. This term should not be confused with the fast electron temperature, it represent the fast electron average energy. These types of curves can be seen through PIC simulation, and some examples are plotted in the section 3.3.1 (see figure 14).

In order to give the maximum amount of energy into the fuel core, we have to generate electrons in a certain range of temperature. If the electrons are too cold, they will not have enough kinetic energy to give. But if they are too hot, they will have so much kinetic energy that their cross-section will be a lot smaller (as this parameter depend on Temperature), and they will pass trough the fuel core without deposing the energy in it. To get the highest absorption rate, the electrons kinetic energy must be between 0,3 MeV and 1,0 MeV. This why it is important to control the ignitor pulse (LFEX pulse) in order to control the fast electrons generated.

1.5 Motivation for using Plasma Mirrors (PM)

Ultra-intense, short pulse lasers are characterized by pulse lengths ≤ 1 ps, much faster than typical plasma expansion time scale ($\propto 100$ ps). This would imply, that short pulse lasers only interact with over-dense

plasma (that we study in the section 2.4). This is not usually the case. Typical short laser pulses are indeed composed by a long ($\sim$ ns), low intensity pedestal, followed by the short, high intensity pulse. The intensity contrast ratio between the short pulse and the pedestal can be as high as $10^7 - 10^{10}$ (depend on the laser system). Nevertheless, for ultra-relativistic laser pulses, the intensity of the pedestal can be of the order of few times 10^{12} W/cm^2. This intensity is high enough to create a plasma expanding into vacuum approximately at the speed of sound c_s. The scale length of the plasma can be defined as $c_s\tau$, where τ represents the length of the pedestal pulse. The short pulse, therefore, before reaching the relativistic critical surface propagates into an under-dense plasma, and can be modified by nonlinear processes, that wee will study in the section 2.3.

However, using Plasma Mirrors can help us to increase the contrast ratio by getting rid of the pedestal. A Plasma Mirror (PM) is an ultra fast optical shutter, rapidly changing its optical properties from almost perfectly transmissive to highly reflective. In the beginning, the PM has a transmission rate of 99,8%. This means that most of the pedestal will go through the PM. But when the main pulse arrives, the mirror get ionized, and the transmission rate drop near 0%. This is because the pulse have enough energy to ionize the surface of the PM, creating a critical density of plasma that reflect incoming beams (this phenomenon is explained in the section 2.1). The process is resumed in the figure 7.

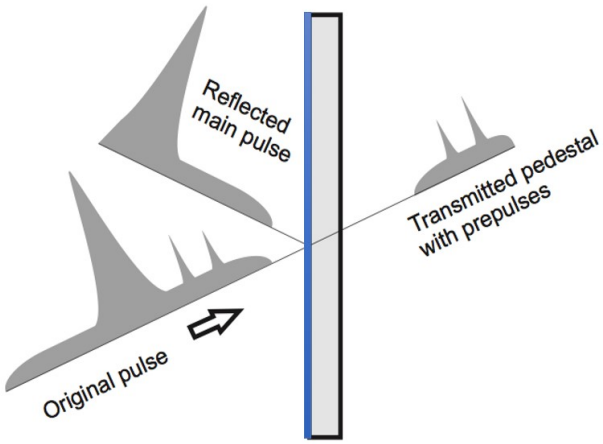

Figure 7: Schematic of the PM work. The pedestal passes through the surface, but the main pulse is reflected because it has enough energy to ionize the surface, and this cause the transmission rate to drop.

By increasing the contrast, we reduce the formation of pre-formed plasma before the target, and so the interaction between the main pulse and the under-dense plasma. With this, it will be easier to generate electron in the energy range where they will be absorbed by the imploding fuel, increasing the heating performance.

During this work, we set up and installed a PM for the LFEX laser in the Institute of Laser Engineering of the Osaka University in Japan. This dissertation will first explain some basis of plasma physics and laser-plasma interactions. Then, we will study the effects of having a pre-formed plasma to proove the interest for using a PM. Finally, we will see how we installed the PM for the LFEX system.

2 Review of theory of laser-plasma interaction

Plasma is one of the four fundamental states of matter, and was first described by chemist Irving Langmuir in the 1920s [3]. It consists of a gas of ions and free electrons. The resulting charged ions and electrons become influenced by long-range electromagnetic fields, making the plasma dynamics more sensitive to these fields than a neutral gas. This is why it is important to make a quick recap on plasma physics and laser-plasma interaction to understand the phenomenon that occurs in a fusion reaction. This physics field require a good understanding of electromagnetism and statistical physics.

2.1 Equations derived from the plasma physics

We start our discussion on the interaction of electromagnetic waves with plasma by introducing a fundamental plasma parameter, the plasma frequency ω_p. Let's consider a plasma initially in equilibrium, with completely stationary ions and electrons positioned in the minima of the electrostatic potential. A small displacement in the position of the plasma electrons will create an electric field acting as are storing force. Once free to move, the energy stored in the electric field will be transformed into kinetic energy of the electrons, accelerated towards the original position. The kinetic energy acquired by the electrons will force them to undergo periodic oscillations around the potential minima. These kind of oscillations are called "Langmuir oscillations", and their proper frequency is the plasma frequency ω_p:

$$\omega_p = \sqrt{\frac{n_e e^2}{m\epsilon_0}} \tag{7}$$

where m is the electron mass, n_e is the number density of electron and ϵ_0 is the permittivity of free space. Let's now consider a high frequency electromagnetic wave propagating in a plasma. From the Maxwell equations and the continuity equation we can obtain the dispersion relation:

$$\omega^2 = c^2k^2 + \omega_p^2 \tag{8}$$

The dispersion relation has several interesting implications. In particular if we consider the group velocity.

$$\frac{\delta\omega}{\delta k} = \frac{c^2}{1 + \frac{\omega_p^2}{c^2k^2}} \tag{9}$$

We can see at at very low frequencies ($ck \ll \omega_p$), only constant frequency waves with $\omega = \omega_p$ can propagate. Being $\frac{\delta\omega}{\delta k} = 0$, no energy or information can be transported in the plasma. At very high frequencies instead $\frac{\delta\omega}{\delta k} = c$ the wave propagates as in vacuum. The plasma frequency therefore, determines the propagation of electromagnetic waves in the plasma. it can be seen as the capability of the plasma electrons to respond to an electromagnetic stimulation. This can be more clearly seen considering again the dispersion relation.

$$\omega^2 - \omega_p^2 = c^2k^2 \tag{10}$$

which implies that an electromagnetic wave with frequency $\omega < \omega_p$, cannot propagate in a plasma, having an imaginary wave vector k. Indeed, if we solve this equation for the wave vector k we obtain:

$$k = \frac{(\omega^2 - \omega_p^2)^2}{c} \tag{11}$$

which assumes imaginary values for $\omega < \omega_p$. The electron density corresponding to this cutoff is called critical density and is given by:

$$n_c = \frac{m\omega^2}{\epsilon_0 e^2} \tag{12}$$

Depending on the intensity of electromagnetic radiation, several are the mechanism that could contribute to the wave damping in regions where the plasma density is above n_c. For low intensities the loss mechanism is related to collisional damping of the wave, due to the excitation of electrons that subsequently lose their energy by collisions with the plasma ions. For higher intensities various absorption mechanisms collisional and collisionless, take place. We will address some of these phenomena, important for the generation of hot electrons in the section 2.4.

2.2 Single electron in a laser field

We should start our discussion on laser plasma interactions by treating the motion of a single electron in a laser field. A focused laser beam can be approximated locally by a linearly polarized wave of amplitude E_0 as:

$$\vec{E}(x,t) = E_0 e^{ikx - i\omega t} \tag{13}$$

$$\vec{B} = \frac{\vec{k}}{\omega} \times \vec{E} \tag{14}$$

The motion of an electron in an electromagnetic (EM) wave obeys the following equation [4]:

$$\frac{d}{dt}(m\vec{v}) = -e(\vec{E} + \vec{v} \times \vec{B}) \tag{15}$$

where m is the particle mass, $-e\vec{E}$ is the electric force and $-e(\vec{v}\times\vec{B})$ is the magnetic force. This expression can be easily corrected for relativistic electron energies by multiplying the mass by the relativistic γ factor. In general a solution $x(t)$ is highly non-linear, depending both on electric and magnetic field. For non relativistic laser intensities the magnetic field can be disregarded, being its magnitude $B = E/v_{\omega/k}$ where $v_{\omega/k}$ is the phase velocity. We therefore find :

$$\vec{v}(x,t) = -i\frac{e}{m\omega}\vec{E}e^{ikx - i\omega t} \tag{16}$$

$$\vec{\delta}(x,t) = -i\frac{e}{m\omega^2}\vec{E}e^{ikx - i\omega t} \tag{17}$$

where $\vec{v}(x,t)$ and $\vec{\delta}(x,t)$ are respectively the electron oscillation velocity and the periodic displacement. An important quantity for future discussions is the cycle-averaged oscillation energy W:

$$W = \frac{1}{4}m\vec{v}^2 = \frac{e^2}{4m\omega^2}E^2 \tag{18}$$

Indicating the velocity of the electron oscillation center as v_0, the energy conservation writes as:

$$E_{kin} + W = \frac{1}{2}mv_0^2 + \frac{e^2}{4m\omega^2}E^2 = const \tag{19}$$

with W representing effectively a potential energy and taking its negative gradient we obtain a force f_p:

$$f_p = -\nabla W = -\nabla\frac{e^2}{4m\omega^2}E^2 \tag{20}$$

called ponderomotive force, and W represents the ponderomotive potential. The ponderomotive force can be considered as a generalization of the radiation pressure. It causes the particle to move towards the area

of the weaker field strength, rather than oscillating around an initial point as it happens in a homogeneous field. This occurs because the particle sees a greater magnitude of force during the half of the oscillation period while it is in the area with the stronger field. We can remark that the charge sign of the particle does not change the direction of the force. This force will be responsible for some strange phenomenon occurring in laser-plasma interactions.

2.3 Laser interaction with under-dense plasma

As we saw in the section 1.5, because high intensity lasers invariably have a pedestal of energy that creates a preformed plasma, the main laser pulse will often have to propagate through a region of under-dense plasma ($n_e < n_c$) before reaching the critical surface where its energy is primarily absorbed. Depending on the properties of the laser itself, the beam can be distorted or modified, and even transfer some fraction of its energy to the under-dense plasma.

2.3.1 Self-focusing and filamentation

The wavefront of the laser beam is not uniform, with regions of varying intensities. In general, the intensity of the laser is higher in the central region. Because of the ponderomotive force that pushes the electrons towards the area of weaker field, the area in in the center of the beam will have a lower plasma density. That lower plasma density will cause the refractive index to increase.

$$n = \frac{k_L c}{\omega_L} = \sqrt{1 - \frac{n_e}{n_c}} \tag{21}$$

As a result, the center part of the beam will travel slower than the external part, bending the wavefront. The curvature produces a focusing effect which increases the intensity even further (see figure 8).

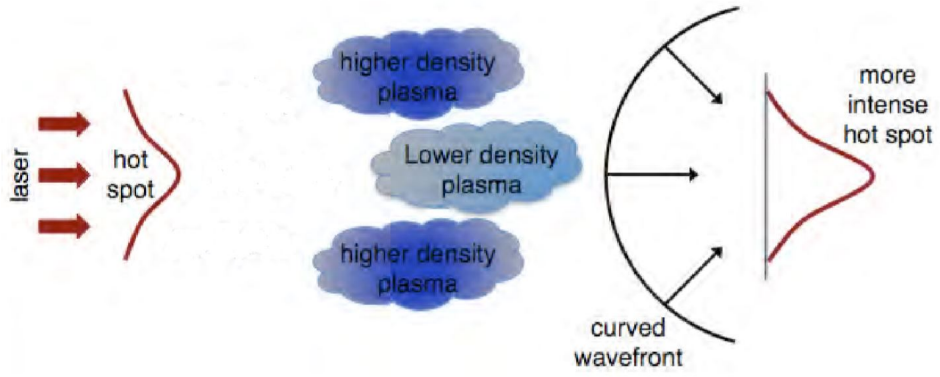

Figure 8: The mechanism behind self-focusing and filamentation caused by the ponderomotive force

Relativistic self-focusing is a similar phenomenon. For relativistic laser intensities, the nonuniform intensity of the laser implies that the electron in the central region will have higher relativistic mass γm, increasing the refractive index in the axial region. This phenomenon have been observed thanks to the PIC simulation done in the section 3, and is shown in the figure 9

Filamentation is when multiple channels are formed with the self-focusing effect. A more complete explanation can be found in the 2002 article of A. Pukhov [5].

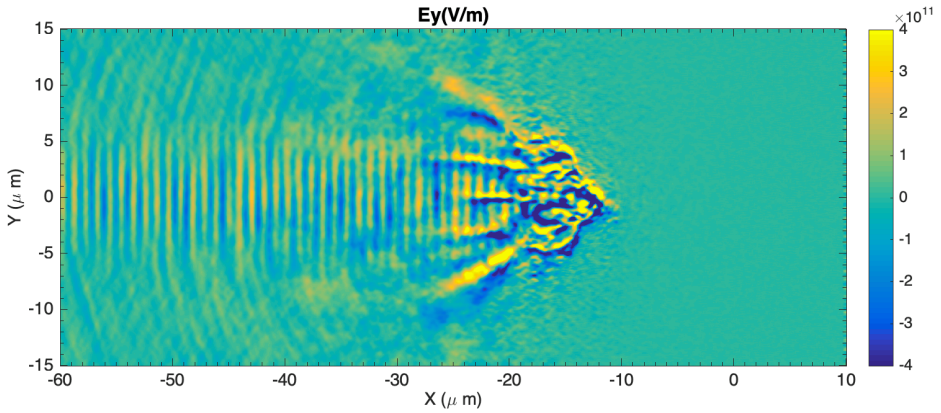

Figure 9: Self-focusing caused by a large pre-formed plasma extension on a high intensity laser ($10^{19} W/cm^2$). This image was done using a PIC simulation described in the section 3.

These effects are not desirable, as they cause the laser to generate fast electrons that have too much kinetic energy ($Ekin > 1MeV$). Also, self-focusing cause the laser to channel through the under-dense plasma, creating a curved critical density surface. Part of the electrons will be accelerated near the normal direction of this surface (especially via vacuum heating/Brunel effect, see section 2.4.2), increasing the electron beam divergence and reducing the heating performance. This effect was observed during the computational study in the section 3.3.2. To avoid this, we need the lowest amount of under-dense plasma before the target, hence the interest of PM.

2.3.2 Inverse Bremsstrahlung

The inverse Bremsstrahlung is the main phenomenon that cause the fuel capsule to absorb the energy of the GEKKO XII laser. At relatively low laser intensities ($10^{12} - 10^{15}\ W/cm^2$), one of the predominant mechanisms of laser energy absorption in plasma is represented by collisions with plasma ions. But first, we should see the process of the Bremsstrahlung. It is an electromagnetic radiation produced by the deceleration of a charged particle when deflected by another charged particle, typically an electron by an atomic nucleus. The moving particle loses kinetic energy, which is converted into radiation (i.e., a photon), thus satisfying the law of conservation of energy.

In opposition, the inverse Bremsstrahlung is the absorption of a radiation by an electron, giving it kinetic energy. The electron particles, which were previously simply oscillating back and forth in the laser electric field, now experience momentum-changing collisions (with other electrons or nucleus). Thus, the laser light effectively gets damped as energy is transferred to these electrons, and the plasma proportionally heats up. This is the effect responsible of the explosion of the fuel capsule resulting of the implosion of the fuel core. The electron-ion collision frequency is given by:

$$\nu_{ei} = \frac{3 \times 10^{-6} Z^2 n_e ln(\Lambda)}{T_e^{3/2}}\ s^{-1} \tag{22}$$

with $ln(\Lambda)$ the Coulomb logarithm and T_e the electron temperature. From 22 we can observe that the collision frequency increases with the plasma density, and decreases with temperature. As consequence, for very high laser intensities, the collision frequency drops due to the very high electron oscillation energy. The collisional absorption remains substantial in case of heavy (high Z) materials, due to the quadratic dependence on Z.

2.4 Laser interaction with over-dense plasma

For very high laser intensities ($> 10^{17}\ W\ cm^2$), the energy carried by the pulse is mainly absorbed at the critical surface. The absorption processes are mainly collisionless, since the collision frequency drops dramatically at very high electron temperatures. These processes lead to the formation of high energetic electron beams, that can propagate through the solid material, far beyond the critical surface, and deposit the laser energy deeper in the target material.

2.4.1 Resonance absorption

Resonance absorption consists in the excitation of plasma oscillations that takes place when a component of the laser electric field is parallel to the plasma density gradient $\vec{E_L} \cdot \vec{\nabla} n \neq 0$ (i.e., when p-polarized light is obliquely incident on a plasma density gradient). The laser light will be specularly reflected at the critical density n_c, and the electric field component tunnels through the critical density, driving a plasma wave in this region. Figure 10 illustrates this process in detail.

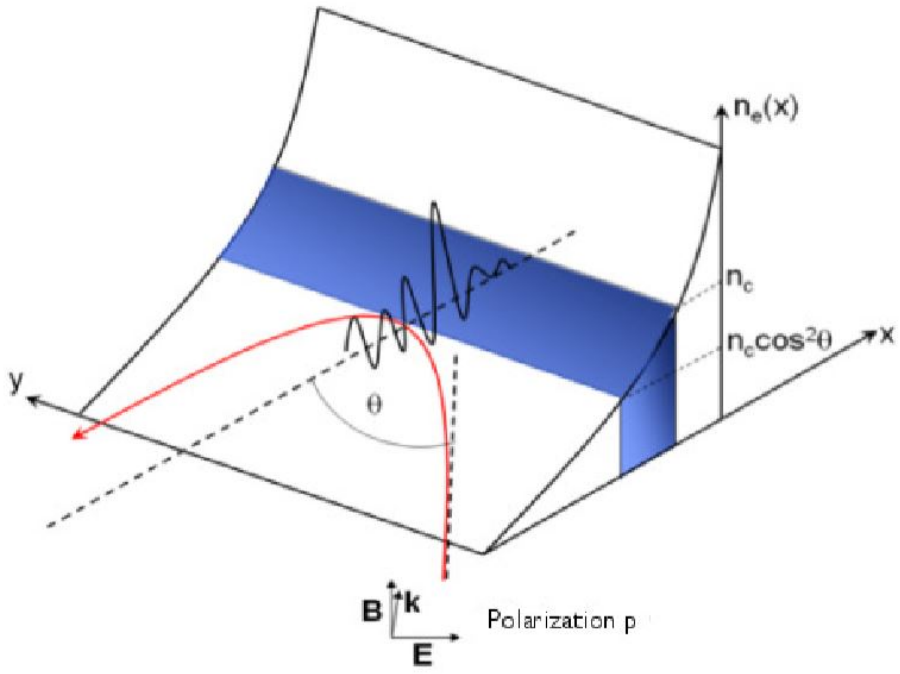

Figure 10: Schematic of resonance absorption where the electric field of the p-polarized laser light is along the same direction as the plasma density gradient. The laser light is reflected at the critical density and a Langmuir wave is driven by the electric field component parallel to the density gradient.

The Langmuir wave (briefly introduced in section 2.1) generated grows for a number of laser cycles and is damped either by collisions (at low intensities) or by electron trapping and wavebreaking (at high intensities), heating the plasma electrons up to hundreds of keV [6]. Resonance absorption will dominate over inverse Bremsstrahlung at high laser intensities (high plasma temperatures) because this absorption persists even when the classical collision frequency, ν_{ei}, is small.

2.4.2 Vacuum heating

Vacuum heating or Brunel absorption was first discussed by F. Brunel in 1987 [7]. This mechanism occurs when the plasma density scale length is smaller than the wavelength of the incident laser light. Because of the steep plasma density gradient, no resonance absorption can take place with this configuration. Nonetheless, an acceleration mechanism occurs, still dependent on the $\vec{E_L} \cdot \vec{\nabla} n \neq 0$ condition, and involving the electrons located at the sharp boundary plasma-vacuum. Because the vacuum-plasma interface is so sharp, electrons near this boundary will be directly exposed to the laser field. The laser electric field can reach unperturbed the steep density gradient, accelerate the electrons into the vacuum over a semi-cycle and re-accelerate them into the plasma in the subsequent semi-cycle. Because the plasma is highly over-dense (i.e., many times n_c), the electric field only penetrates to a skin depth ($\sim c/\omega_p$), so the electron can continue on into the target until its energy is eventually absorbed through collisions. With this phenomenon, we can have a peak absorption of 70 % [8]. However, at higher intensities and shorter scale lengths, the absorption saturates to around 10-15 %. This phenomenon is a predominant form of relativistic electrons generation and and heating process for FI.

2.4.3 J x B heating

For laser light intensities exceeding the relativistic limit ($\sim 10^{18}\ W/cm^2$), the motion of the electron in the laser field cannot be described solely by the action of the electric field. The $\vec{v} \times \vec{B}$ term of the Lorentz force becomes non negligible, and accelerates the electrons in the laser propagation direction with $2\omega_L$ frequency (ω_L being the laser frequency). A free electron in an intense laser field undergoes oscillations parallel and perpendicular to the wave vector $\vec{k}$, and the global trajectory is simply a composition of the two oscillations. Very similarly to the vacuum heating process, depending on the phase of the oscillating electrons, they may gain energy from the laser electromagnetic wave, decouple, and be propelled into the over-dense plasma. The number of electrons that escape the wave and get propelled into the over-dense plasma depends on the strength of the oscillating force. This phenomenon is also a predominant form of heating process during FI.

2.5 Electron beam transport through plasma

In the previous sub-section we saw how we can generate supra-thermal electrons (with kinetic energies of hundreds of keV to several MeV) that can transport the energy far beyond the critical density. Here, we focus our attention on the properties of the fast electron beams, and on the physics related to their transport in the solid density of the plasma.

2.5.1 Conversion efficiency

The LFEX laser intensity is clearly above the relativistic limit, reaching peak values of $\sim 10^{19}\ W/cm^2$. At these intensities, a significant amount of the laser energy is transferred into fast electrons. Many experiments have been performed to measure the fast electron conversion efficiency (i.e., the amount of energy transferred from the laser to the fast electrons). In the article by J.R. Davies [9], we can see that the laser energy absorption increases with $I\lambda^2$ and increases for lower density plasma and for non-normal incidence. Notice that here we are here talking about overall energy absorption and not absorption in fast electrons. Indeed the fast electron absorption inferred in laser-solid experiments is consistently lower than the total absorption inferred in both experiments and numerical modeling and this difference increases with $I\lambda^2$. This may be the result of energy transfer to outwards ion acceleration (i.e., plasma expansion). From these measurements, it would appear that the maximum fast electron absorption that could be achieved is approximately 50%, value still adequate for FI.

2.5.2 Stopping power

As the fast electrons propagate through the target material, the particles will feel a combination of both collisional and collective effects. The collisional stopping power is due to binary collisions with plasma electrons and ions resulting in the loss of energy by inelastic scattering with electrons and radiative losses due to Bremsstrahlung emission (briefly introduced in section 2.3.2). The total collisional stopping power can be written as:

$$\left(\frac{dE}{ds}\right)_{tot} = \left(\frac{dE}{ds}\right)_{coll} + \left(\frac{dE}{ds}\right)_{rad} \tag{23}$$

Collisional effects will dominate in cases where the total number of hot electrons is relatively small and the average hot electron energy is very large. However, a fast electron beam propagating in matter can be described by a current $I(A)$, with a current density $J(A/cm^2)$, and the total electron current is quite large. If we consider a $\tau \approx 700fs$ laser pulse with average intensity $\sim 5 \times 10^{19} W/cm^2$ and total energy of $E_L \approx 150J$, and assuming a conversion efficiency of $\eta_{eff} \approx 30\%$, the fast electron current can be estimated as:

$$I \approx \frac{E_L \eta_{eff}}{T_{hot}\tau} \approx 25 \times 10^6 A \tag{24}$$

This current can physically not propagate as it is much greater the Alfven limit [10]. The Alfven current ($J_A = 15000\gamma\beta$) represents the largest current that can propagate in vacuum or in a conductive medium. A higher current cannot propagate anymore due to the self-generated magnetic field action on the beam, which turns the electrons back. However, experimental results show that such a high current does in fact propagate, which forces to make the assumption that this current is balanced by a a second, counter-propagating return current, composed by background plasma electrons.

$$J_{tot} = J_{fast} - J_{ret} \approx 0 \tag{25}$$

The return current is composed of a large number of slow electrons, attracted by the density of ions concentrated where the fast electrons have been generated. Due to their much lower velocity, the return current electrons undergo collisions with background ions much more efficiently than fast electrons, or in other words, are more sensitive to the plasma resistivity. Because the value of J_{tot} is not 0, there is a generation of an electric field opposed to the fast electron transport, resulting in the so-called collective stopping power. The higher the plasma resistivity, the higher the stopping power will be. This is why in the next section we will study the plasma resistivity.

2.5.3 Plasma resistivity

Plasma resistivity is due to the collision of moving electrons with the background ions. However, the estimation of this quantity can be quite difficult. If we follow the Drude model [11], we can define the resistivity as:

$$\eta = \frac{m\nu}{e^2 n_e} \tag{26}$$

where ν is the electron-ion collision frequency and n_e the plasma electron density. The knowledge of η relies on the knowledge of these two parameters ν and n_e. The difficulty is that it's hard to estimate these quantities for a wide range of temperatures and densities. However, Lee and More [12] developed a model based on the linearization of the Boltzmann equation, in stationary state (Maxwellian distribution) and in the limit of small temperature gradients and weak electric field. A Lee and More resistivity curve for solid density and compressed Al is represented in figure 11.

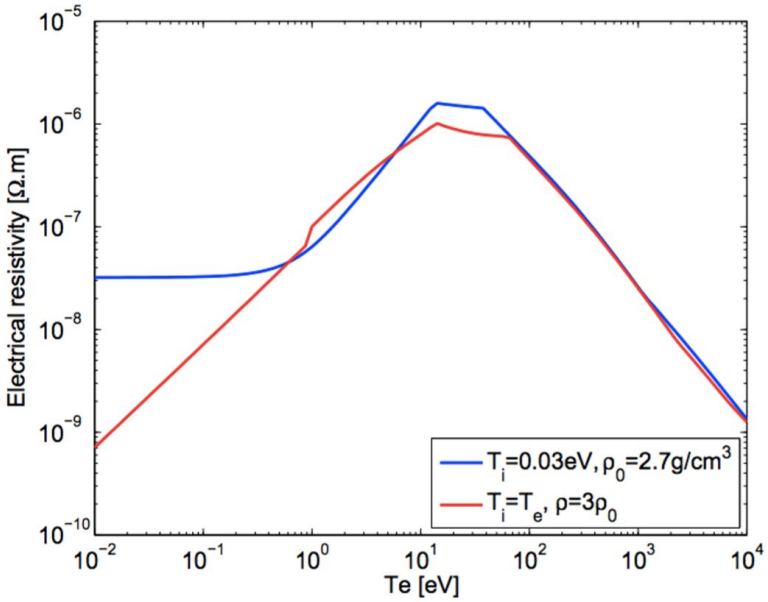

Figure 11: Electrical resistivity curve for solid density ρ_0 ($2.7g/cm^3$) and compressed Al density $3\rho_0$ calculated from the Lee and More model over a wide range of temperatures (from 10^{-2} to 10^4 eV). This graph come from [13].

We see on this curve that for very hot electrons (i.e., $T_e > 10^2 eV$), the resistivity drops. This is due to the fact that the cross-section is smaller for relativistic electrons, thus, decreasing the collision frequency and so the plasma resistivity (see equation 26). This is why the return current face resistance in comparison with the fast electron current in the section 2.5.2.

3 Computational study

Computer simulations are carried out for three main reasons: (1) to understand the consequences of fundamental physical laws, (2) to help interpret experiments (it can provide detailed information which is difficult to measure) and (3) to design and predict new experiments. We are not interested on the motion of a single particle, but in the collective phenomena that plasma displays. These phenomena, such as waves, reconnection, anomalous resistivity, instabilities, transport and heating can only be seen by considering a large number of particles and how they manage to come together. The motion of these particles is highly non-linear and far out of equilibrium due to relativistic particle motion. Non-linearity of plasma is caused by several interdependent processes occurring in plasma, which constantly feedback to each other and modify plasma properties. These complicated phenomena require kinetic models such as the particle-in-cell model (PIC).

3.1 Particle-In-Cell model (PIC)

The PIC method refers to a technique used to solve a certain class of partial differential equations, and were already in use as early as 1955 [14]. It simulate a plasma system by following a number of particle trajectories in the phase space (i.e., $\vec{x_i}$ and $\vec{v_i}$). As the number of particles involved is to big, we use "macroparticles", but we keep the same charge/mass ratio so the plasma frequency is invariant (see equation (7) in the section 2.1). However, even if the number of particles simulated is much smaller than in reality ($10^3 - 10^{11}$), it is enough to capture the essential physic.

It is too expensive to calculate inter-particles forces directly. So we divide the phase space into cells, and for the ones that contain a particle, we calculate the charge density and the electrical current (i.e., ρ_{ij} and J_{ij} from x_k and v_k in 2D). From these, we can calculate E_{ij} and B_{ij} by solving the Maxwell's equations, and then find the force F_k that will apply on the particle. If multiples particles are in the same cell, they will all feel the same force, and this is one of the reason why we need a good resolution by decreasing the cells dimensions. We update the particles position in the phase space with a time step that we arbitrary choose, and we restart the process. This method is resumed in the figure 12.

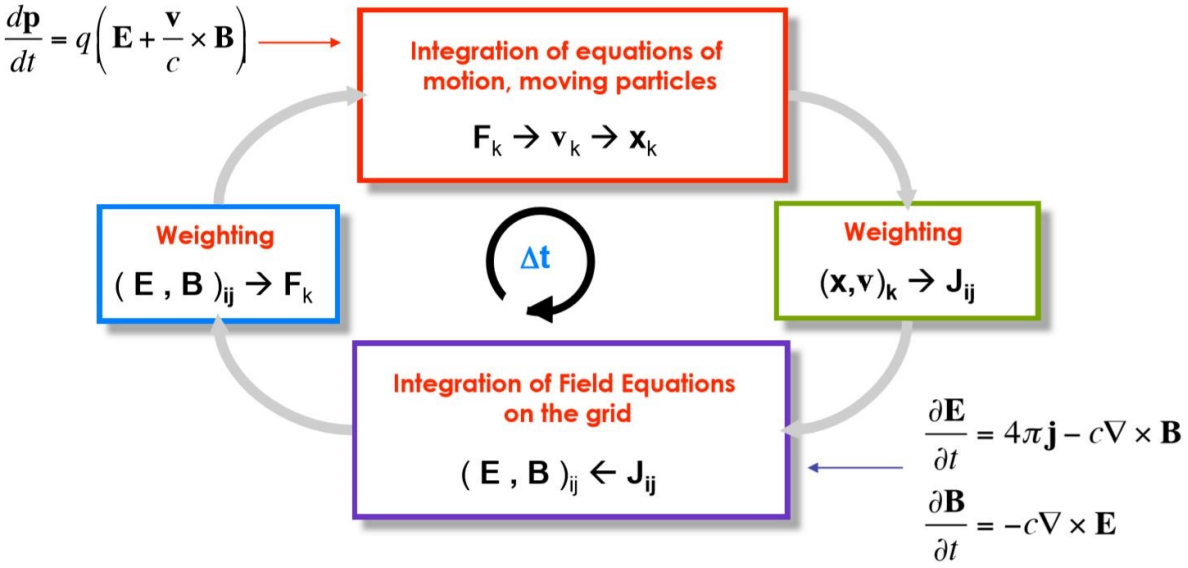

Figure 12: The simple and straightforward PIC Scheme.

To compensate the smaller number of particles used, we give them a finite-size that will greatly reduce the close-range collision. However, PIC model is not collision-less, and can still be used to test collision operators. However, the simulation that we will run will be collision-less as it require less computing power.

3.2 2D simulation of high intensity laser interaction with pre-formed plasma

This work was done during the second month of the internship. To understand the consequences of having a pre-formed plasma before the target, we can use a PIC simulation using a software called EPOCH. This software is used to run simulations of high intensity laser-plasma interaction. Instead of directly coding the simulation, the user go through an input deck where he can change the initial parameters of his simulation. For our research project, we want to simulate a solid target (that we approximate with a very high density plasma $n_{solid} \sim 40n_c$), and a pre-formed plasma using an exponentially increasing plasma density (see figure 13). This pre-formed plasma is defined by the equation.

$$n = n_{solid}e^{x/L} \tag{27}$$

with L the pre-formed plasma scale length (i.e., the steepness of the plasma density gradient). To see the effect of the pre-formed plasma on fast electron generation, we will run five simulation, each time using a different value of pre-formed plasma scale length (L = $0.1\mu m$, $0.5\mu m$, $1\mu m$, $2\mu m$, $5\mu m$). Each time L increase, the pre-formed plasma extension before the target will increase.

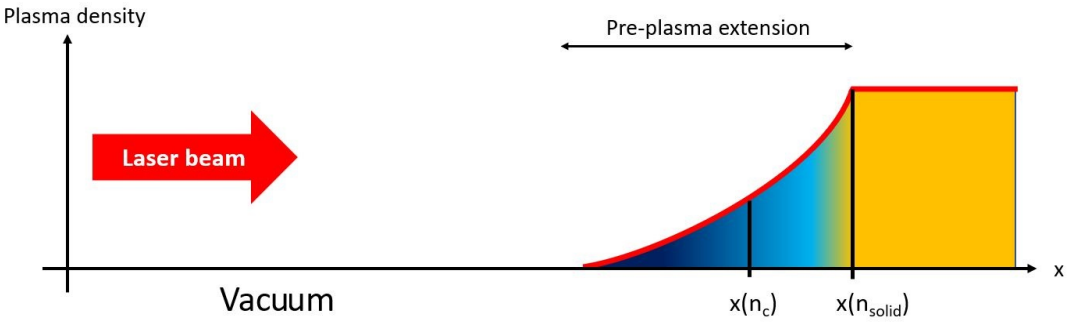

Figure 13: Graphical representation of the simulation that we ran. The plasma density increase exponentially until it reach a solid density.

The laser will be an electromagnetic wave propagating from the left border of the simulation. This beam will represent the LFEX pulse, and will be characterised by an intensity of 10^{19} W/cm^2, and a wavelength of 1.054 μm.
A small super-computer was needed in order to run these simulations, each one taking $\sim$ 3 hours to finish using 20 processor cores. On a normal laptop using 8 processor cores, a single simulation takes $\sim$ 11 hours.

3.3 Results

To analyse the data from the simulations, we used Matlab codes that take the .sdf data files to give us the plot of the result. Each of these diagnostics are discussed in this sub-section.

3.3.1 Effect on conversion efficiency

The conversion efficiency is a value between 0 and 1 that describe how much of the laser energy is transferred to the relativistic electrons in the form of kinetic energy. The higher this value, the more we

generate relativistic electrons, thus increasing the heating performance. For each simulation, we can plot the conversion efficiency for a certain electrons kinetic energy range. Results are written in the table 1.

$0.3 < E_{kin} < 20$ MeV		$0.1 < E_{kin} < 0.5$ MeV	
L (μm)	Conv. Eff.	L (μm)	Conv. Eff.
0.1	0.2027	0.1	0.1984
0.5	0.1833	0.5	0.1614
1	0.1866	1	0.1085
2	0.4292	2	0.1238
5	0.6008	5	0.1422

Table 1: Conversion Efficiencies for high kinetic energy electrons and for low kinetic energy electrons.

For a high energy range, the conversion efficiency is much higher for long pre-formed plasma scale length (L), but for a lower energy range, the conversion efficiency increase when L is shorter. Plots of the electron energy spectrum of the two energy range for each value of L is presented in the figure 14. In this figure, the amount of high energy electrons generated is much higher for longer pre-formed plasma scale length, confirming the previous result on conversion efficiency. The generation of high energy electrons can be explained by the fact that the laser travel longer through under-dense plasma where fast electrons are being generated thanks to the ponderomotive force. Also, the data shows that self-focusing of the laser beam is occurring before it reaches the critical density. Because of this phenomenon, electrons are facing a higher intensity beam and absorb more energy. Beside, having a shorter pre-formed plasma scale length can generate more low energy electrons. This is good because these electrons energy will be better absorbed by the imploded fuel core and give an overall better heating performance. However, the conversion efficiency is not the only parameter that determine the heating performance.

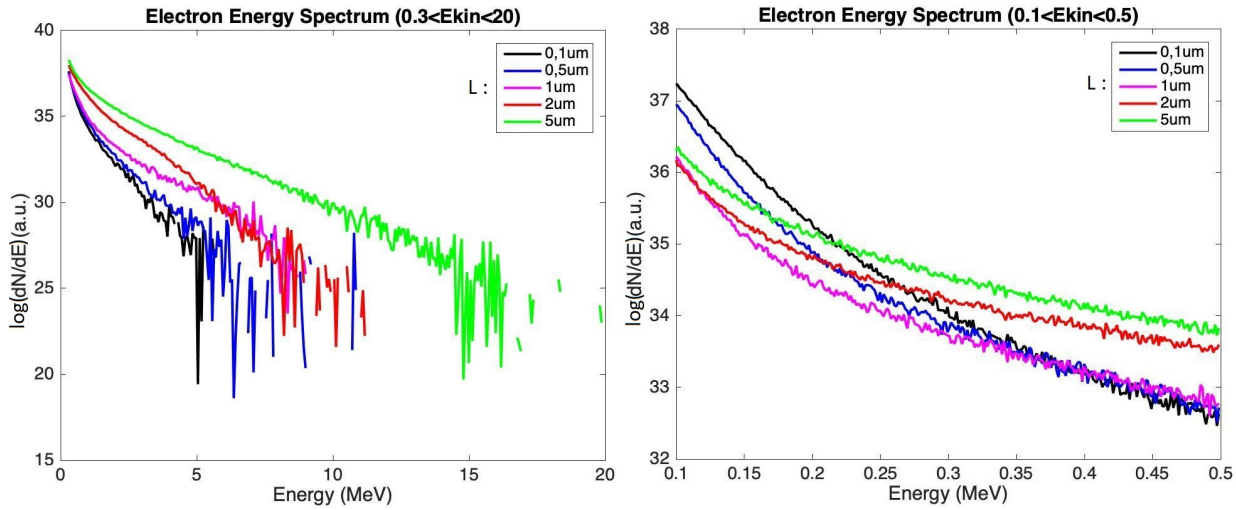

Figure 14: Electron energy spectrum between 0.3 MeV and 20 MeV, and between 0.1 MeV and 0.5 MeV for each value of L. The graph represent the electron density (in logarithmic scale) as a function of the kinetic energy. A longer L generate more high energy electrons, a shorter one generate more low energy electrons.

3.3.2 Effect on fast electron divergence

If we want the electrons kinetic energy to be absorbed by the fuel core, the angle of the electron emission (in comparison with the laser axis) must be as low as possible. This mean that the electrons angular distribution is also a very important parameter. With the data from the EPOCH simulations, we can plot the density of electron as a function of their angle of emission (see figure 15).

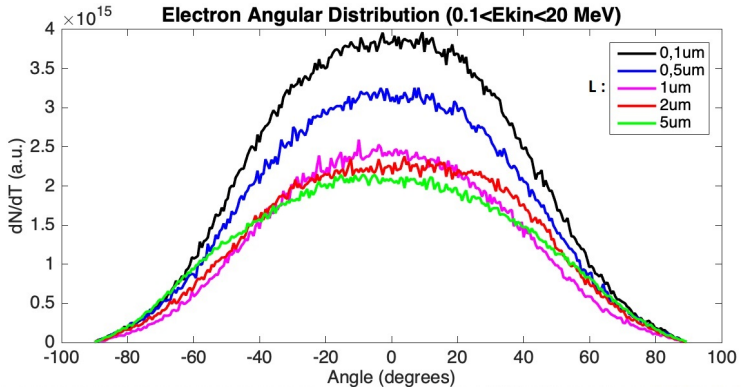

Figure 15: The graph represent the electron density as a function of the angle of emission for each value of L. The electron beam divergence is much narrower for short pre-formed plasma scale length.

Even if a longer L generate more high energy electrons, their angular distribution is much broader, meaning that less electrons will collide with the fuel core. We see that for 0.1 μm scale length, the angular distribution is narrower. Several factors can explain the lower electron beam divergence. Firstly, there is less interactions between the under-dense plasma and the laser. Laser channelling in lower density plasma occurs, thus creating a curved critical surface. Part of the electrons (especially via vacuum heating/Brunel effect) will be accelerated near the normal direction of this surface as shown on the figure 16.

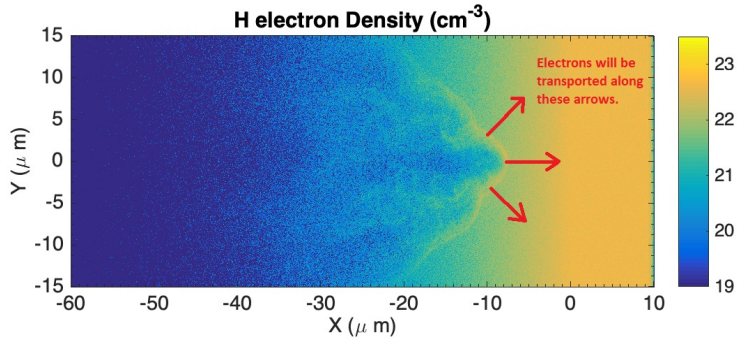

Figure 16: The laser channel through the under-dense plasma, creating a curved critical surface and generating fast electrons normal to this surface because of the vacuum heating. Here, $L = 5\mu m$.

Also, there is a phenomenon that can be observed if we look at the magnetic intensity field on the figure 17. For short pre-formed plasma scale length, we can see filaments due to Weibel instabilities [15].
As a result, the electrons momentum will be anisotropic (i.e., will depend on the direction) as they will move along the lines drawn by the magnetic filamentation, thus reducing the electron beam divergence. This effect was unexpected during the experiment, and further research on these instabilities will be done by the Fusion Plasma Science group in the future. Finally, the electron generation distance from the target increase with L (see figure 18). The further the electrons are being generated, the bigger the beam diameter

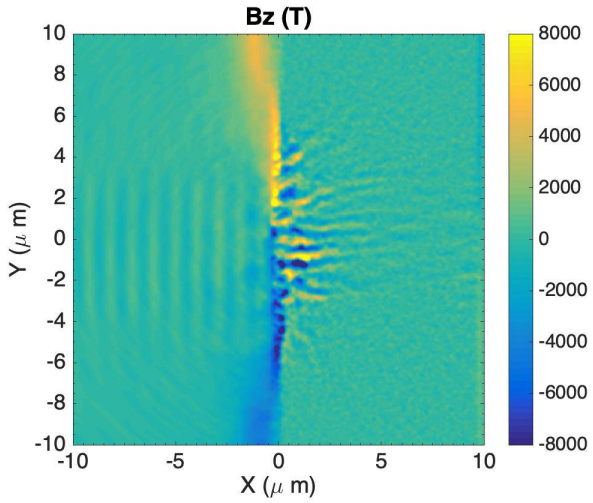

Figure 17: Weibel instabilities causing the magnetic field to filament when the laser beam hit the critical density. The electrons will move along the lines, reducing the electron beam divergence. $L = 0.1\mu m$.

will be near the target.

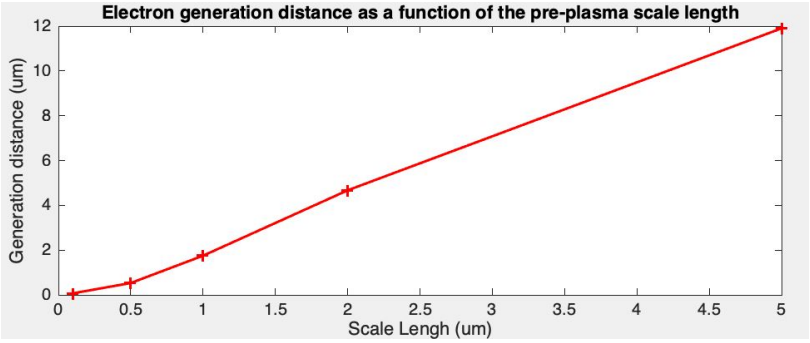

Figure 18: Fast electrons generation distance from the solid target as a function of L.

3.4 Conclusion on heating performance

For good heating performance, we need high conversion efficiency in a certain energy spectrum ($\sim 0,2MeV < E_{kin} < 1MeV$) and low electron beam divergence. Overall the conversion efficiency is higher for longer L. However, for short L the conversion efficiency is higher for low energy electrons (i.e., the ones that can be better absorbed by the fuel core). Furthermore, a shorter L reduce the electron beam divergence and the electron generation distance. These 2D simulations proves that using a PM can improve the heating performance of the LFEX laser by reducing the pre-formed plasma scale length.

4 Setup and Installation of the Plasma Mirror (PM)

4.1 Introduction

Now that we saw how a PM can help us improving the contrast of the LFEX laser, we need to install and setup it for the fusion chamber at the ILE. This was an optical calibration work, done in a place called the Alignment Station (AS). This manipulation, crucial for the success of the experiment, is detailed in this section. All this work was done during the first month of the internship, before the the declaration of the state of emergency in Japan.

4.1.1 Constraints

Before we start working on the PM, we need to get a look at the constraints we have to deal with. Indeed, because of the infrastructure of the fusion chamber, we have to be aware of some limitations:

- It is impossible to align the PM from inside the chamber. The chamber diameter at the ILE is only 2 meters, and we cannot get inside it.
- It is impossible to verify the PM focusing from inside the chamber. Same reason.
- With the PM inserted, it is very difficult to align targets with complex geometry in the right position.

This is why we are doing all the calibration work from outside the chamber, in the AS. However, the fact that we don't work directly in the chamber will add some steps for the installation of the PM:

1. Setup a LFEX skeleton on the AS
2. Make a one to one reference between the AS target chamber center and the real one.
3. Move the platform from the AS to the chamber and verify the target position.

Most of these steps could not be finished during the internship because of the Coronavirus outbreak.

4.2 Work at the Alignment Station (AS)

4.2.1 Target Chamber Center (TCC)

The TCC is a point in 3D space that is arbitrary defined by two cameras, perpendicular to each other. This point will then remain for the rest of the experiment. Is role is to make the one to one reference between the AS and the chamber. Indeed, once we placed the target in TCC, and made all the optical calibrations, we just have to move the platform from the AS to the chamber where a real TCC is defined by other cameras. If needed, we can move the platform or the LFEX laser in order to adjust the position and orientation of the optical setup.

The role of the author was to verify the alignment of the cameras, and to define TCC using a fake target and the images of the cameras on a computer screen (see figure 19). Actuators on the cameras helped us to precisely define the point in 3D space.

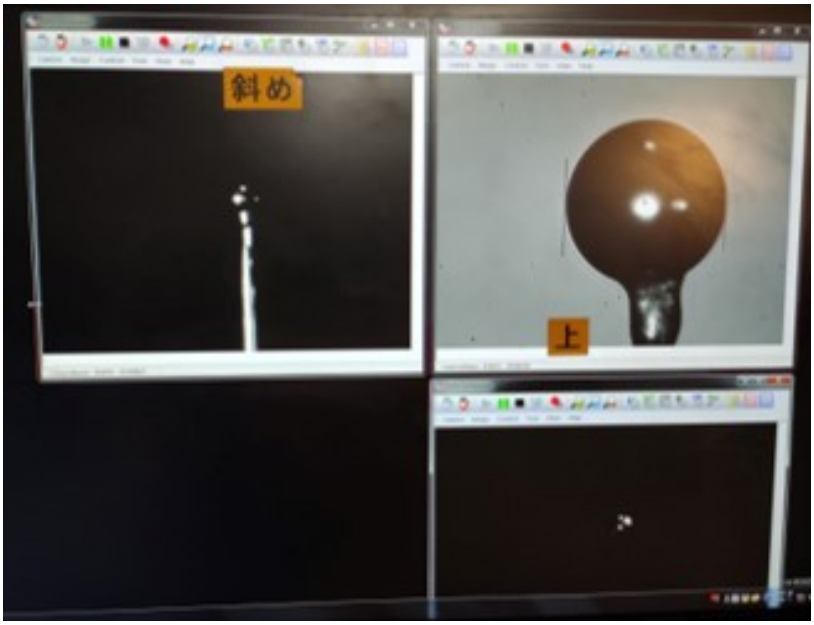

Figure 19: Photography of the computer screen with a fake target in TCC. The image on the top left and bottom right are from the cameras that defined TCC. The image on the top right come from a third camera with a microscope lens used to observe the target.

4.2.2 LFEX skeleton

Because we are not working in the fusion chamber, we need to reproduce the LFEX beam in order to make the optical calibration. For that, we setup an LFEX skeleton with a He-Ne laser. After defining the axis of the laser beam (we verify that the beam arrive with an angle of incidence of 0 degrees on the target, thanks to autocollimation), we setup the skeleton line as shown on the figure 20.

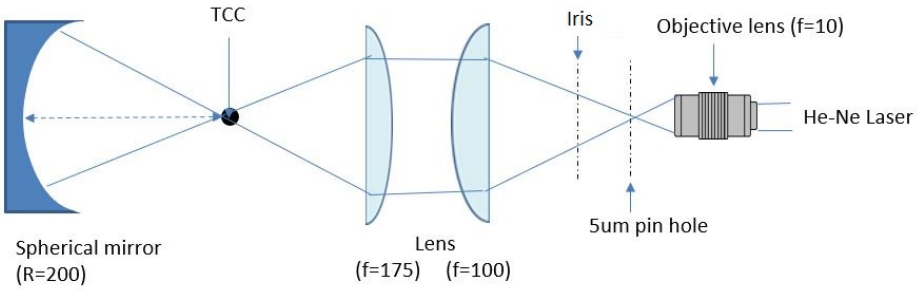

Figure 20: Design of the LFEX skeleton line for the AS.

The microscope lens and the pin-hole are used to clean up the beam and have a homogeneous wave front. The iris is used to change the clear aperture of the beam, in order to match the f-number of the LFEX. The f-number of an optical system is the ratio of the system's focal length to the diameter of the entrance pupil. The AS system's focal length is fixed and equal 175mm (because of the second lens), so in order to change the f-number, we have to control the diameter of the beam with the iris. The f-number of the LFEX is equal to 5. After going through the first lens, the laser pulse re-focused in TCC. In the figure 21 is shown a photography of the setup of the LFEX skeleton on the AS.

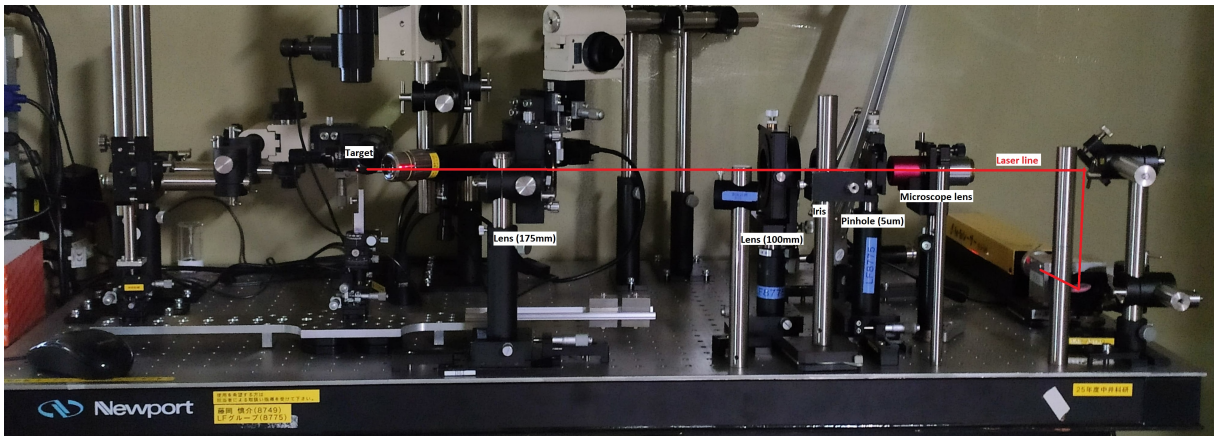

Figure 21: Photography of the AS with the LFEX skeleton setup. The red line represent the laser path.

4.2.3 Mirror Alignment

The beam coming out from the LFEX skeleton will not be directly focused on TCC, but will be focused 4mm below, and reflected by the spherical PM into the target. This is due to the way the platform and the target are inserted in the chamber. All diagnostics are aligned in re-entrant geometry looking at TCC and this cannot be modified. Moreover, the GEKKO XII beams for target compression can be focused only on TCC. The platform will be fixed thanks to a magnetic base on a surface coming from the bottom of the chamber, and the target will be injected from the top. By focusing the laser down, we are sure that the incoming beam will not collide with the support of the target. By tilting the mirror up, we are able to re-focus the laser beam 4mm up, into the target.

In the section 4.1.1, we saw that it was impossible to verify the plasma mirror focusing from inside the chamber. However, we will need to verify if the LFEX beam will correctly hit the target. For that, we use a custom made double pin-holes of 0.1mm diameter, 4mm apart from each other. The incoming laser beam should be focused on the first pin-hole below, then the beam is be reflected by the spherical PM and pass through the second pin-hole located in TCC. If this is achieved, we should be able to observe the light coming out of the top pinhole, and so the direction of the laser is verified. After that, we remove the double pin-holes from the support, inject the target and shoot !

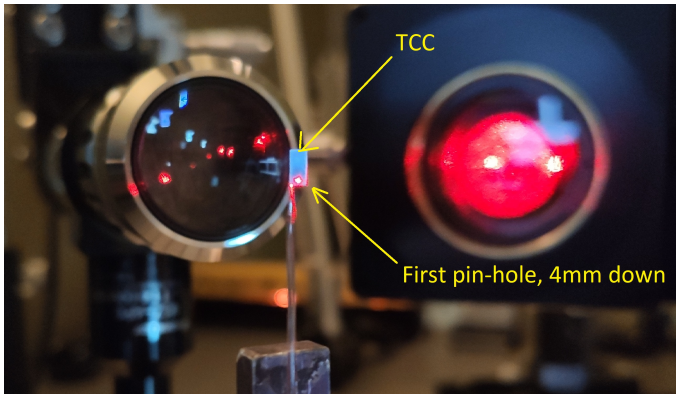

Figure 22: Photography of the double pin-holes on the AS. The laser passes through the first pin-hole below TCC. The mirror was not installed yet, so we don't see the light going through the second pin-hole.

5 Conclusion and perspective

5.1 Summary and conclusions

5.1.1 Fast electron generation and transport

After seeing the basics of FI and identifying the problematic of the LFEX pedestal in the introduction, the section 2 gave us all the important theoretical tools to understand the physical phenomenon that we can observe in FI study. The interaction between high intensity laser (i.e., $I > 10^{18}\ W/cm^2$) and over-dense plasma show that most of the fast electrons are being generated thanks to the vacuum heating and J x B heating process. However, many effects like the self-focusing or filamentation can be observed if under-dense plasma is on the way of the LFEX laser beam. And because the pedestal generate a pre-formed plasma in front of the target (i.e., under-dense plasma), these effects can appear if we don't use a PM.

5.1.2 Effect of pre-formed plasma for fast electron generation

The effect of pre-formed plasma for fast electron generation have been studied through computational study using a PIC code 2D simulation in the section 3. Long pre-formed plasma scale length cause the laser to self-focus, increasing the electrons energy and the beam divergence. Futhermore, a smaller pre-formed plasma scale length generate electron nearer the target and cause Weibel instabilities that helps reducing the beam divergence. Clearly this section demonstrates that the presence of long pre-formed plasma can significantly alter the laser-solid interaction at relativistic intensities, and thus hamper the prospects of FI. This prove that using a PM can greatly improve the heating performance of the LFEX laser. We also saw how the GEKKO XII laser can make the fuel implode thanks to the inverse Bremsstrahlung, and how the electrons are being transported from the target to the imploded fuel core.

5.1.3 Setup and Installation of the plasma mirror

Finally, the section 4 shows the setup and installation of the PM. In order to succeed, we had to find solutions for the infrastructural constraints. The use of an alignment station in order to properly setup and calibrate the plasma mirror was the first step to achieve the experiment at the ILE, and can hardly be transposed to another laboratory. Because it is the first step, it was very important to be as accurate as possible, and a lot of time and effort was spent to make sure that all the optical instruments was precisely installed. If not, a lot of labour in the future will be wasted.

5.2 Future Work

The computational work that were conducted made great strides in the understanding of the effect of pre-formed plasma on fast electron generation. The discovering of Weibel instabilities due to the short pre-formed plasma scale length will be a future subject of study for the Fusion Plasma Science group. Additional experiments can be conducted to further explore these phenomena. If more computing power is accessible, one of the obvious extension of this work would be to investigate the problem with a better resolution, or in a 3D case.

The experiment just started, and a lot of work is still do be done in order to see the impact of the PM for relativistic electrons generation. After installing the PM on the AS, we will have to make the one to one reference between the station and the fusion chamber. This will be done using the TCC and the double pinholes. The future work will be focused on the installation of the platform and the PM in the fusion chamber.

Even though advances have been made in this area, several unknowns are still present that prevent mankind to achieve nuclear fusion, which require further investigation. FI is an advanced scheme for inertial confinement fusion with the potential for a lower ignition threshold, less stringent implosion symmetry requirements, and higher gain over central hot spot ignition. If realized, FI may help promote the viability of inertial fusion as a clean and safe energy source.

5.3 Personal review

I presented a small fraction of the experimental and theoretical experience accumulated during the three months of this internship. Nevertheless, these manipulations and simulations played an important role in my scientific formation. I gained a lot of experience, and I will remember three important lesson for my future works:

1. In a big laboratory such as the ILE, with many people from different group working together, it is very important to communicate with everyone. By presenting your progress, telling if any modification was made, or just by giving ideas, it is much easier to detect an issue or to improve the experiment. Having a weekly meeting and good contact with your team is necessary in these type of facilities.

2. Planning and organisation is the key to be able to run such big experiments. It would be impossible to realise fusion science if we didn't agreed with everyone on the dates and schedules. We must know where and when we are going before starting our journey.

3. It is very important to keep the laboratory clean and in order. A lot of time where lost looking for a specific item or tool. Taking the time to put back the unused object in its place can save us more time in the future, when we will be looking for it. This lesson seems basic, but I think it is important to keep it in mind.

I am very happy to have had the opportunity to work at the ILE, with the Fusion Plasma Science group. This internship convinced me that fusion science was the research field for which I want like to dedicate my life to.

Besides all of these experiences, this three months internship was the opportunity to improve my English, and to discover the Japanese culture and traditions.

Annexes

Codes

Listing 1: Input deck for a pre-formed plasma scale length of 0.1um

```
begin:control
    nx = 2005
    ny = 334*3
    npart = 400 * ny * 50
    # final time of simulation
    t_end = 1800 * femto
    # size of domain
    x_min = -60 * micron
    x_max =  10* micron
    y_min = -15 * micron
    y_max = 15 * micron
    smooth_currents = T
    dlb_threshold = 0.9
    stdout_frequency = 2
end:control

begin:boundaries
    bc_x_min = simple_laser
    bc_x_max = open
    bc_y_min = open
    bc_y_max = open
end:boundaries

begin:constant
    lambda0 = 1.054 * micron
    omega = 2 * pi * c / lambda0
    pden = 40 * critical(omega)
    # xii will determine the pre-formed plasma extension.
    xii = -1 * micron
    xi = 0 * micron
    xf = 10 * micron
end:constant

begin:species
    name = deuteron1
    charge = 1.0
    mass = 1836.2*2
    frac = 0.5
    temp_ev =200
    # This is where we determine the pre-formed plasma scale length.
    density=if((x gt xii)and(x lt xi),pden*exp(x/(0.1*micron)),density(deuteron1))
    density=if((x gt xi)and(x lt xf),pden,density(deuteron1))
end:species
```

```
begin:species
    name = electron1
    charge = -1.0
    mass = 1.0
    frac = 0.5
    temp_ev =200
    density = density(deuteron1)
end:species

begin:laser
    boundary = x_min
    intensity_w_cm2 = 1e19
    lambda = lambda0
    profile = gauss(y,0*micron,4*micron)
    t_profile = gauss(time,900*femto,500*femto)
end:laser

# Probe (extraction plane) that records all the electrons
# that cross the plane (for each electron records px,py,pz)
# and that we will use to determine the hot electron spectrum.

begin:probe
    name = fast_electron
    point = (7* micron, 0 * micron)
    normal = (1.0, 0.0)
    ek_min = 0
    ek_max = -1
    include_species:electron1
    dumpmask = restart
end:probe

begin:output
    # number of timesteps between output dumps
    dt_snapshot = 200 * femto
    # Number of dt_snapshot between full dumps
    full_dump_every = 1
    restart_dump_every = 1
    force_final_to_be_restartable = T
    dt_average = 7.08e-15
    # Properties at particle positions
    particles = full
    particle_weight = full
    # Properties on grid
    grid = always
    ex = always + average + snapshot
    ey = always + average + snapshot
    ez = always
```

```
    bx = always
    by = always
    bz = always + average + snapshot
    jx = always
    jy = always
    jz = always
    ekbar = always + average + species
    charge_density = always + average
    number_density = always + species
    temperature = always + average + species
    absorption = always
    total_energy_sum = always
    # extended io
    distribution_functions = always
    particle_probes = always
end:output
```

Commentary

This is the input.deck code for a pre-formed plasma scale length of 0.1 μm. This code is easy to navigate through, as it does not show all the code used for the simulation, but only the conditions to the limits. We can see that for this scale length, the pre-formed plasma extension is $xii = -1$ μm. In order to make another simulation, with a different pre-formed plasma scale length, we have to change this value (for example, $0.1 \rightarrow 0.5$) and the pre-formed plasma extension (same example, $-1 \rightarrow -5$).

References

[1] J.D. Lawson. Some criteria for a power producing thermonuclear reactor. *Proc. Phys. Soc. B*, 70(6), 1957.

[2] M.H. Key. Status of and prospects for the fast ignition inertial fusion concept. *Physics of Plasmas*, 14(055502), 2007.

[3] I. Langmuir. Oscillations in ionized gases. *Proceedings of the National Academy of Sciences of the United States of America*, 14(8):627, 1928.

[4] F.F. Chen. *Introduction to Plasma Physics and Controlled Fusion.* 2006.

[5] A. Pukhov. Strong field interaction of laser radiation. *Reports on Progress in Physics*, 66(1), 2002.

[6] A Modena, Z Najmudin, AE Dangor, CE Clayton, KA Marsh, C Joshi, Victor Malka, CB Darrow, C Danson, D Neely, et al. Electron acceleration from the breaking of relativistic plasma waves. *Nature*, 377(6550):606–608, 1995.

[7] F. Brunel. Not-so-resonant, resonant absorption. *Phys. Rev. Lett.*, 59:52–55, Jul 1987.

[8] P. Gibbon. *Short pulse laser interactions with matter*. World Scientific Publishing Company Singapore, 2004.

[9] J.R. Davies. Laser absorption by overdense plasmas in the relativistic regime. *Plasma Physics and Controlled Fusion*, 51(1):014006, 2008.

[10] H. Alfvén. On the motion of cosmic rays in interstellar space. *Physical Review*, 55(5):425, 1939.

[11] P. Drude. Zur elektronentheorie der metalle. *Annalen der physik*, 306(3):566–613, 1900.

[12] Y.T. Lee and R.M. More. An electron conductivity model for dense plasmas. *The Physics of fluids*, 27(5):1273–1286, 1984.

[13] A. Morace. Study of fast electron transport and energetic proton generation at high laser intensity and application to fast ignition. 2013.

[14] F.H. Harlow. A machine calculation method for hydrodynamic problems. *Los Alamos Scientific Laboratory report*, 1955.

[15] Erich S Weibel. Spontaneously growing transverse waves in a plasma due to an anisotropic velocity distribution. *Physical Review Letters*, 2(3):83, 1959.

List of Figures

1 Binding energy per nucleon versus atomic mass number A. 4
2 Fusion cross sections for various fusion reaction versus ion temperature. The DT fusion cross section is the largest at low temperatures. 5
3 Indirect drive (left) and Direct drive (right). 6
4 Fuel assembly for CHS ignition (isobaric assembly), and Fast Ignition (isochoric assembly). 7
5 Gain estimates for direct-drive Fast Ignition targets from a simple analytic model compared with numerically modeled CHS ignition disigns for NIF. The FI gain curves are labeled with fuel density, energy, and $I\lambda^2$ in the ignitor laser beam, assuming a wavelength of 530nm. [2] 8
6 Au cone target from the ILE, Osaka University. 8
7 Schematic of the PM work. The pedestal passes through the surface, but the main pulse is reflected because it has enough energy to ionize the surface, and this cause the transmission rate to drop. 9
8 The mechanism behind self-focusing and filamentation caused by the ponderomotive force . 12
9 Self-focusing caused by a large pre-formed plasma extension on a high intensity laser ($10^{19}W/cm^2$). This image was done using a PIC simulation described in the section 3. 13
10 Schematic of resonance absorption where the electric field of the p-polarized laser light is along the same direction as the plasma density gradient. The laser light is reflected at the critical density and a Langmuir wave is driven by the electric field component parallel to the density gradient. 14
11 Electrical resistivity curve for solid density ρ_0 ($2.7g/cm^3$) and compressed Al density $3\rho_0$ calculated from the Lee and More model over a wide range of temperatures (from 10^{-2} to 10^4 eV). This graph come from [13]. 17
12 The simple and straightforward PIC Scheme. 18
13 Graphical representation of the simulation that we ran. The plasma density increase exponentially until it reach a solid density. 19
14 Electron energy spectrum between 0.3 MeV and 20 MeV, and between 0.1 MeV and 0.5 MeV for each value of L. The graph represent the electron density (in logarithmic scale) as a function of the kinetic energy. A longer L generate more high energy electrons, a shorter one generate more low energy electrons. 20
15 The graph represent the electron density as a function of the angle of emission for each value of L. The electron beam divergence is much narrower for short pre-formed plasma scale length. 21
16 The laser channel through the under-dense plasma, creating a curved critical surface and generating fast electrons normal to this surface because of the vacuum heating. Here, $L = 5\mu m$. 21
17 Weibel instabilities causing the magnetic field to filament when the laser beam hit the critical density. The electrons will move along the lines, reducing the electron beam divergence. $L = 0.1\mu m$. 22
18 Fast electrons generation distance from the solid target as a function of L. 22
19 Photography of the computer screen with a fake target in TCC. The image on the top left and bottom right are from the cameras that defined TCC. The image on the top right come from a third camera with a microscope lens used to observe the target. 24
20 Design of the LFEX skeleton line for the AS. 24
21 Photography of the AS with the LFEX skeleton setup. The red line represent the laser path. 25
22 Photography of the double pin-holes on the AS. The laser passes through the first pin-hole below TCC. The mirror was not installed yet, so we don't see the light going through the second pin-hole. 25

List of Tables

1 Conversion Efficiencies for high kinetic energy electrons and for low kinetic energy electrons. 20